Supporting Information

Differential Photothermal and Photodynamic Performance Behaviors of Gold Nanorods, Nanoshells and Nanocages under Identical Energy Conditions

Yanlin Feng[a, b], Yun Chang[a, c], Xiujuan Sun[a], Yan Cheng[a], Runxiao Zheng[a, b], Xiaqing Wu[a, b], Li Wang[d], Xiaomin Ma[d], Xi Li[d], and Haiyuan Zhang[a, b, c]**

[a]Laboratory of Chemical Biology, Changchun Institute of Applied Chemistry, Chinese Academy of Sciences, Changchun 130022 (P.R. China);

[b]University of Science and Technology of China, Hefei, Anhui 230026 (P.R. China);

[c]University of Chinese Academy of Sciences, Beijing 100049 (P.R. China);

[d]School of Chemistry and Life Science, Changchun University of Technology, Changchun 130012 (P.R. China)

* Correspondence to: Haiyuan Zhang, E-mail: zhangh@ciac.ac.cn.

Table S1 Hydrodynamic sizes and Zeta potentials of naked and *p*Au NRs, NSs, and NCs in DMEM cell culture medium.

Au nanostructures	Hydrodynamic size (nm)	Zeta potential (mV)
NRs	78.8 ±4.0	- 0.5 ±0.2
NRs-PEG	101.5 ±4.4	- 6.4 ±0.2
NSs	128.4 ±5.8	- 5.1 ±0.1
NSs-PEG	131.1 ±5.0	- 14.8 ±0.2
NCs	99.4 ±4.3	- 14.1 ±0.5
NCs-PEG	127.4 ±6.9	- 17.4 ±0.2

Table S2 Parameters for photothermal conversion efficiency calculation.

Parameters	NRs	NSs	NCs
τ_s	349.2	353.9	360.5
hS	0.02	0.02	0.02
OD	1	1	1
10^{-OD}	0.1	0.1	0.1
I (W)	1.3	1.3	1.3
ΔT (K)	17.8	18.6	18.9
T_{max}(K)	48	48.8	49.1
η/%	29.3	30.2	30.1

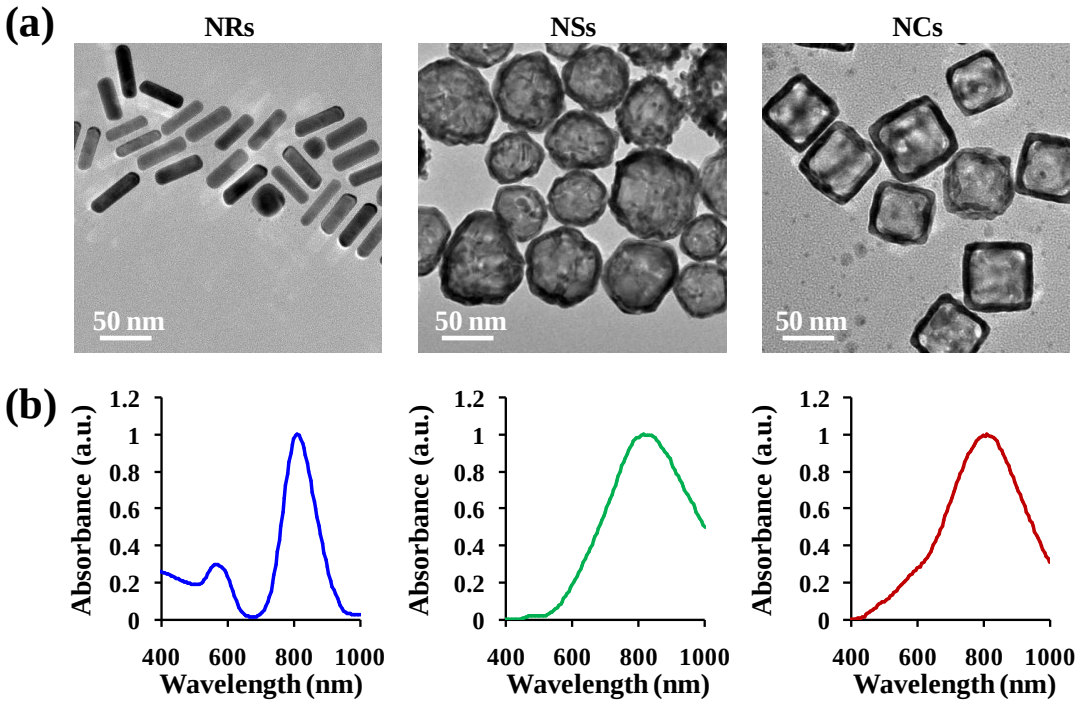

Fig. S1 (a) TEM images of *p*Au NRs, NSs, and NCs. (b) UV-Vis spectra taken from aqueous suspensions of *p*Au NRs, NSs, and NCs.

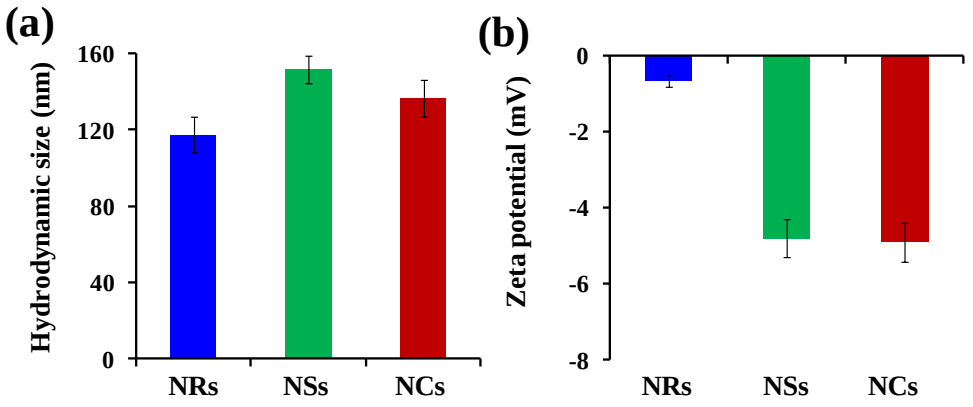

Fig. S2 Hydrodynamic sizes and zeta potentials of *p*Au NRs, NSs, and NCs in water.

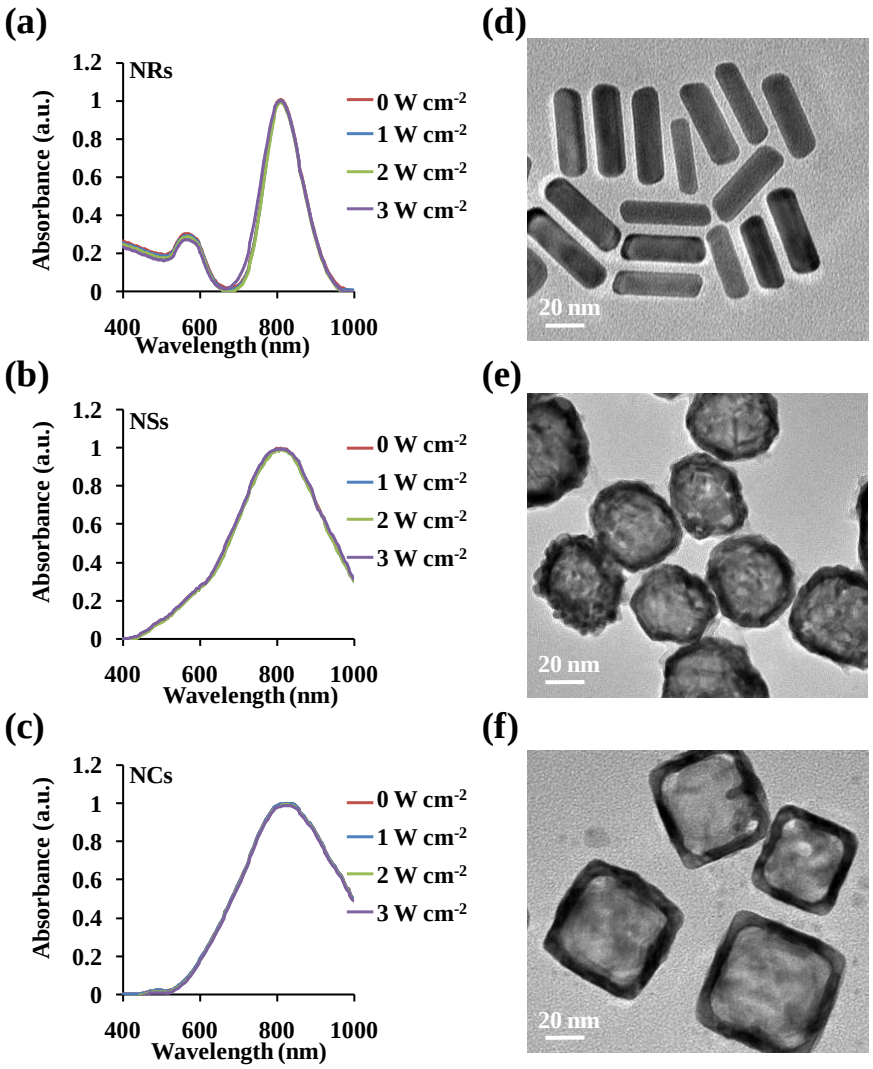

Fig. S3 Photostability of *p*Au NRs, NSs, and NCs under 808 nm laser irradiation. UV-Vis spectra of *p*Au NRs (a), NSs (b), and NCs (c) aqueous suspensions after 808 nm laser irradiation for 10 min at power densities of 1, 2, and 3 W cm^{-2}, respectively; TEM images of *p*Au NRs (d), NSs (e) and NCs (f) after 808 nm laser irradiation (3 W cm^{-2}, 10 min).

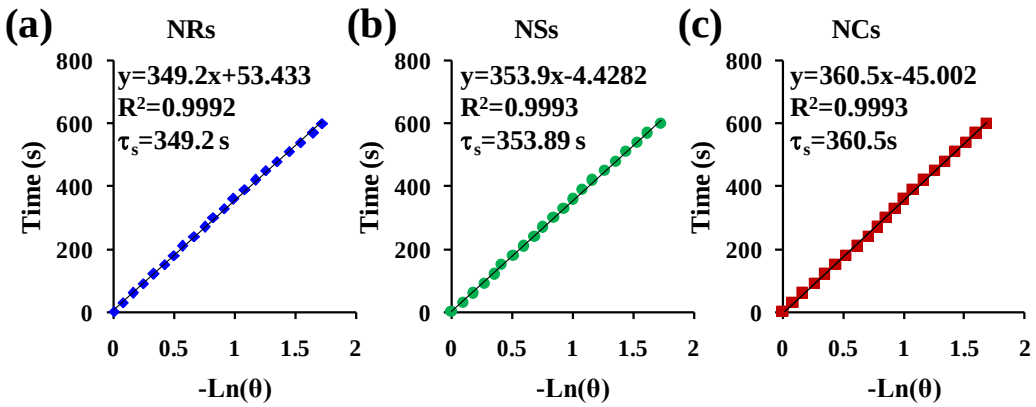

Fig. S4 Plot and linear fit of time versus negative natural logarithm of the temperature increment for the cooling rate of *p*Au NRs (a), NSs (b), and NCs (c).

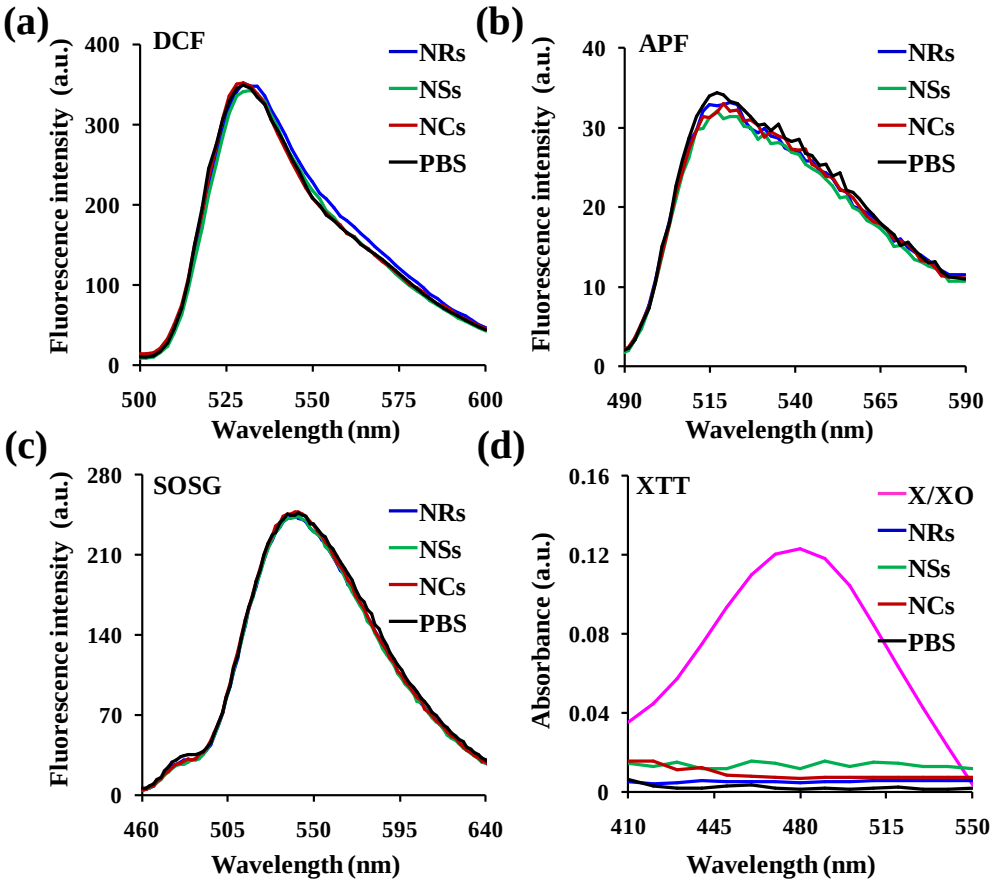

Fig. S5 ROS generation of *p*Au NRs, NSs, and NCs in dark condition. (a) DCF fluorescence; (b) APF fluorescence; (c) SOSG fluorescence, and (d) XTT absorbance in PBS incubated with *p*Au NRs, NSs, and NCs (OD = 1.0) without 808 nm laser irradiation. Xanthine/xanthine oxidase (X/XO) was used as a positive control in XTT assay.

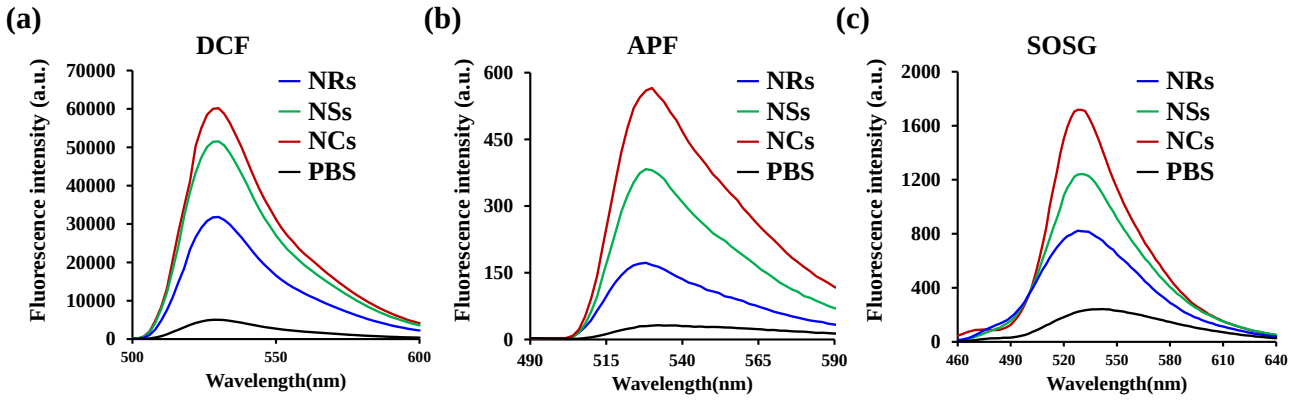

Fig. S6 Assessment of ROS generation ability of *p*Au NRs, NSs, and NCs under NIR laser irradiation with the same concentration (40 μg mL^{-1}) under 808 nm laser irradiation for 10 min at a power density of 0.75 W cm^{-2}. (a-c) DCF, APF, and SOSG fluorescence spectra in PBS incubated with *p*Au NRs, NSs, and NCs (40 μg mL^{-1}).

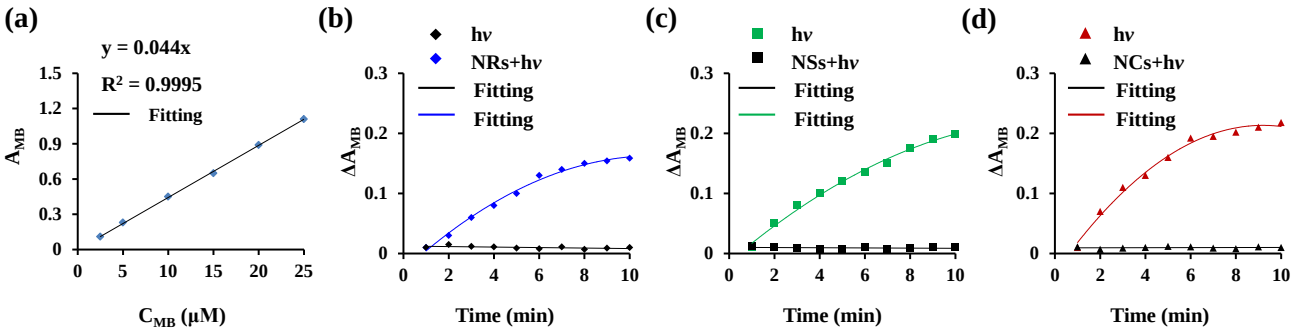

Fig.S7 Quantitative measurements of HO• generation by MB as the reporter probe. (a) Concentration dependent absorbance intensity of MB at 664 nm. Discoloration of MB (ΔA_{MB}) in the presence of Au NRs (b), NSs(c) and NCs (d) or absence of Au nanostructures as a function of irradiation time under NIR irradiation.

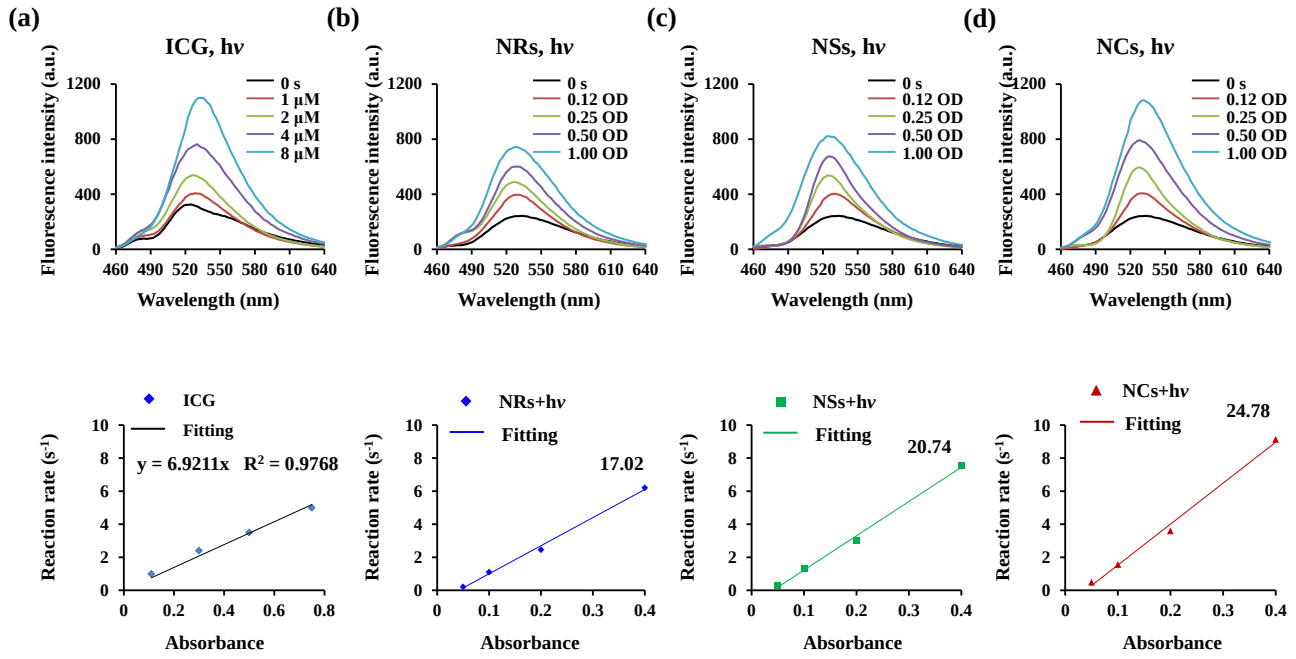

Fig.S8 Quantitative measurements of $^1O_2$ by using SOSG reporter probe. Fluorescence enhancement of SOSG accompanying reaction of 6.0 μM SOSG with $^1O_2$ generated from ICG or AuNCs at different concentrations. (a) ICG under NIR irradiation; Au NRs (b), NSs(c) and NCs (d) under NIR irradiation at 0.75 W cm^{-2} for 10 min (upper), and the relevant reaction rates as a function of ICG or Au NRs, NSs or NCs absorbance (lower).

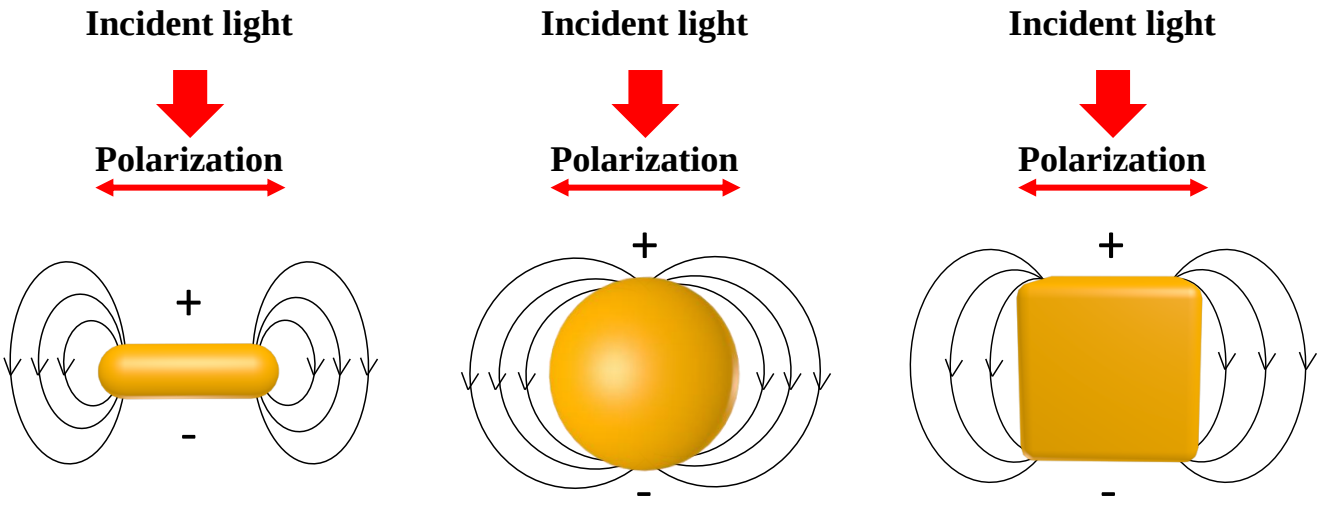

Fig. S9 Scheme shows the uneven electric field distribution and enhancement in the contour plot of Au NRs, NSs and NCs.

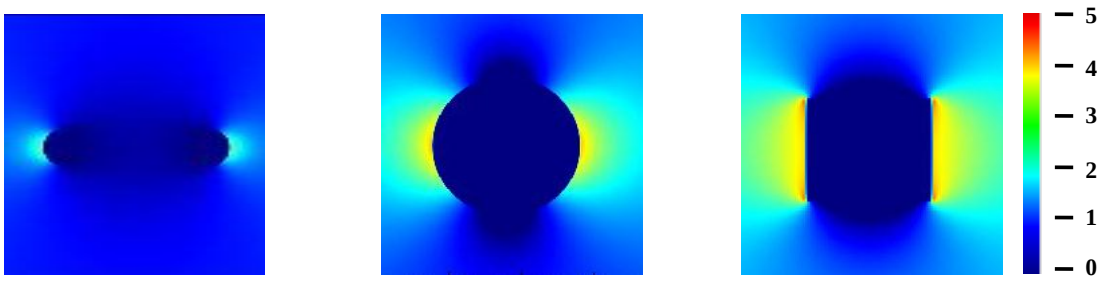

Fig.S10 FDTD calculations for the electric field distribution and enhancement ($|E|/|E_0|$) contours of *p*Au NRs, NSs and NCs at 808 nm excitation.

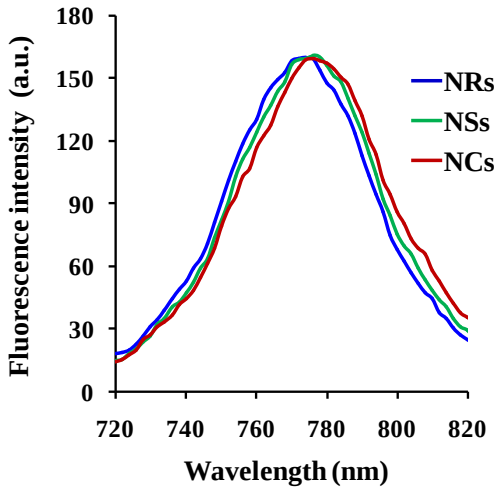

Fig. S11 Fluorescence intensities of Cy-7 labeled *p*Au NRs, NSs, and NCs (OD = 1.0).

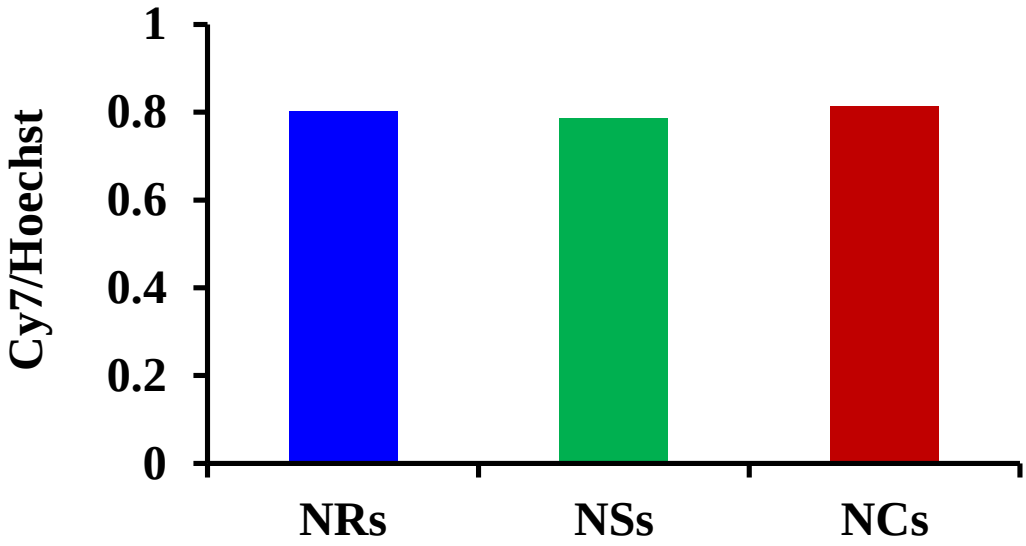

Fig. S12 The ratio of the intensity of Cy7 (Red color) and Hoechst (Blue color) of each image in Fig. 5b. The intensity of Cy7 (Red color) and Hoechst (Blue color) were acquired by Image J Software.

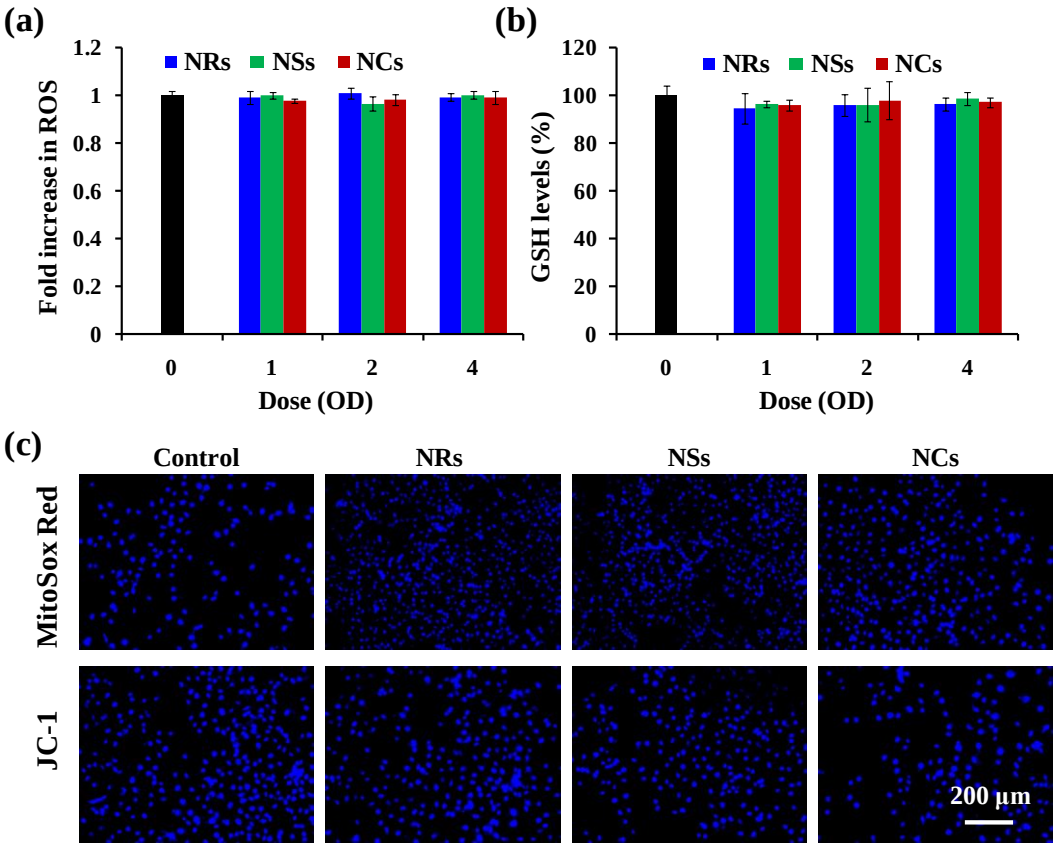

Fig. S13 Cellular ROS, GSH, mitochondrial superoxide generation and membrane potential levels induced by *p*Au NRs, NSs, and NCs without 808 nm laser irradiation. (a) Intracellular ROS levels accessed by ROS-Glo; (b) Intracellular GSH levels accessed by DTNB; (c) Mitochondrial superoxide generation (Mitosox Red, red) and membrane potential (JC-1, green) analysis accessed by fluorescence microscope with 20×objective. Cell nuclei (blue) were stained with Hoechst 33258.

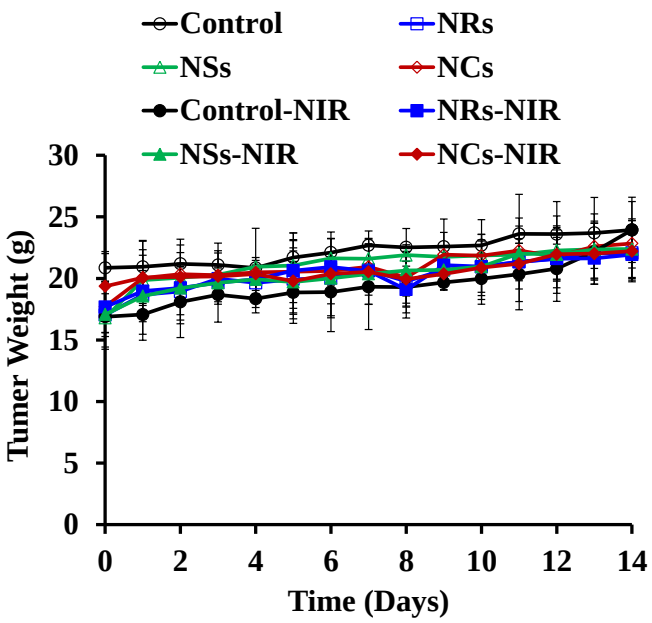

Fig. S14 Body weights of mice from different groups during the treatment period.